Machine Vision and Applications (2010) 21:811–824
DOI 10.1007/s00138-009-0221-z

ORIGINAL PAPER

An advanced auto-inspection system for micro-router collapse

Der-Baau Perng · Yen-Chung Chen

Received: 18 March 2007 / Revised: 21 March 2008 / Accepted: 1 August 2009 / Published online: 12 September 2009

Abstract In this paper, we propose an auto-optical inspection (AOI) system that can inspect micro-router (router) collapse automatically. The router is a tool used to cut a printed circuit board (PCB). A few types of defects could occur in the routers and cause unexpected damage to the PCBs. Among these defects, collapse is the most critical defect that must be detected. Currently, router manufacturing companies rely on human inspectors to control the router quality. We first extract the silhouette edges and associated features (peaks and valleys) of a router's silhouette image by computer vision technique. Then, these silhouette edges and associated features are used to reconstruct a set of 2D isograms that correspond to the router surface. Finally, a pattern recognition method is devised to identify and classify some features of the pattern in the 2D isograms. In this study, two types of routers with different diameters are used for inspection experiments. There are 15 routers of each type. The experimental results reveal that the proposed AOI system can robustly and successfully detect the collapse of diamond-patterned routers with different sizes. The successful detection rate is above 96%. The proposed AOI system can assist in determining the quality of the routers.

Keywords Micro-router · Machine vision · Auto-optical inspection

D.-B. Perng · Y.-C. Chen
Department of Industrial Engineering and Management, National Chiao-Tung University, 1001, University Rd., HsinChu 30010, Taiwan
e-mail: perng@cc.nctu.edu.tw

Y.-C. Chen (✉)
No. 1001, University Rd., HsinChu 30010, Taiwan
e-mail: aaron1229@gmail.com

1 Introduction

The quality of a printed circuit board (PCB), which is an essential element for most electrical products, significantly affects the quality of the electrical products associated with it. To produce a high-quality PCB, the quality of the router, which is a tool used for cutting PCBs, is an important factor. The diameter of a micro-router is as small as 0.6 mm and it has diamond-cut geometry (Union Tool). The side view of the router is illustrated in Fig. 1a. In fact, the diamond-cut geometry surface of a router is the router's blades, which are formed by six and seven interwoven spiral-valley routes in opposite directions, as shown in Fig. 1b. Hence, this type of router is also known as a "diamond-patterned router." The completeness of each blade is a criterion for router quality control. Figure 2 shows two images of a collapsed router. The collapse of the blade would occur when it is machined. When a collapsed router is used for PCB cutting, some unexpected abnormality on the PCB edge will occur and the PCB's life will be affected. Hence, it is the most serious defect that must be detected.

Router manufacturers rely on human inspectors for router quality control. Human inspectors utilize electronic microscopes with adjustable fiber optic illuminators and their judgment to identify the position and damage level of the collapse. However, because the collapse is inherently embedded in the interwoven spiral blades of the router, it is very difficult for humans to inspect such collapse on the router. For example, a router with a diameter of 1.0 mm and a length of 5 mm consists of nearly 40 blades; the area of a blade is approximately $0.4\,\text{mm}^2$. A collapsed area larger than $0.01\,\text{mm}^2$ is a serious defect, and inspectors find it very difficult to detect such an area. Therefore, an advanced system for router auto-inspection has been developed. However, it is difficult to design a lighting system that can provide sufficient and

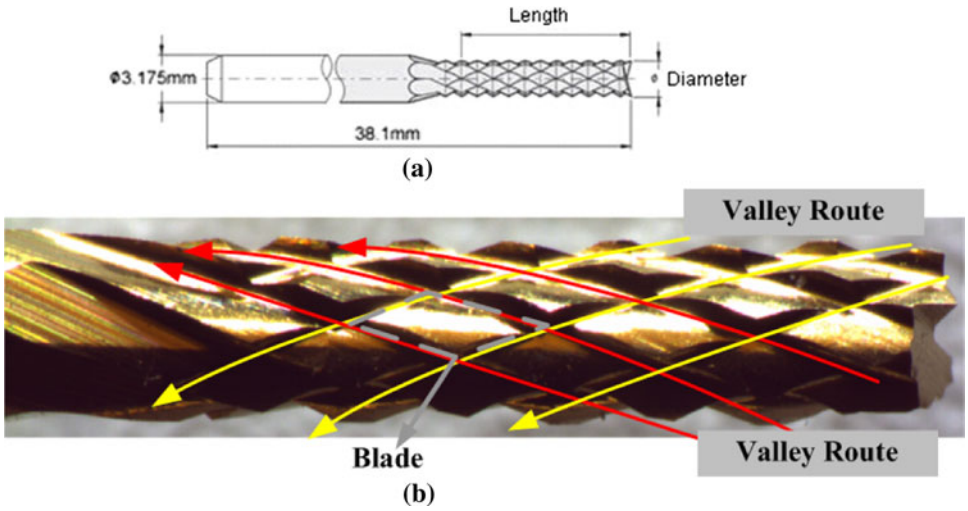

Fig. 1 **a** The side-view graph of a router. **b** Diamond-patterned blades formed by interwoven spiral valley routes in opposite directions

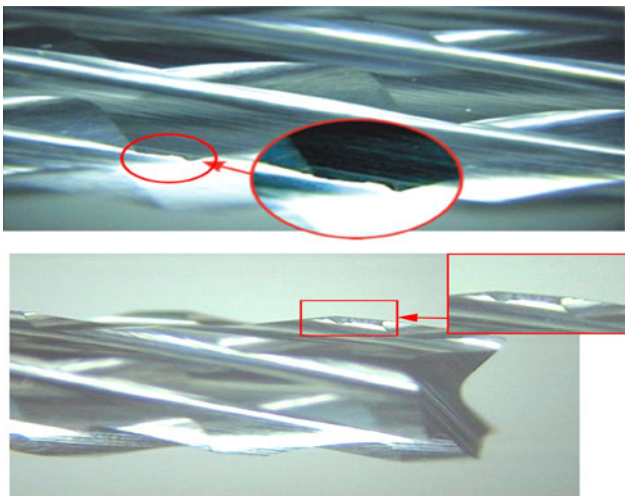

Fig. 2 Two sample collapse images of a diamond-patterned router

uniform illumination on the router's diamond-patterned surface. We use a program-controlled rotational fixture to hold the router and a backlighting system to highlight the silhouette edge of the router. We first extract a sequence of silhouette images of the router by rotating the fixture in steps of 1°. Then, this sequence of silhouette images is used to reconstruct a set of 2D isograms. Because the obtained features correspond to that of the blade contours of the router, which form a specific pattern in the isograms, this pattern is used for router collapse inspection. Finally, a pattern recognition method is devised to identify and classify these patterns. This paper is organized as follows. In Sect. 2, we review some related studies. The hardware system and software algorithms of the proposed auto-optical inspection (AOI) system are described in Sect. 3. The experimental results of the AOI system are described and discussed in Sect. 4. The conclusions and some suggestions are provided in Sect. 5.

Fig. 3 A side-view image of a micro drill

2 Literature survey

2.1 Micro-drill inspection

Currently, there is no report on the inspection of micro-router defects. However, we have found some related studies on the inspection of a micro-drill, which is used to create holes on the PCB [9,10,12,17]. Figure 3 shows a side view of the micro-drill.

Although the silhouette image or the surface appearance of the micro-drill is similar to that of a router, we still observe some differences. The surface pattern of the micro-drill corresponds to that of a unidirectional spiral blade.

2.2 Surface reconstruction from a sequence of 2D images

Some studies use a sequence of 2D images to reconstruct the 3D surface of an object or a 3D pseudo object. These 2D images can be obtained by the structure lighting method [1]; Laser Design), moire grating method [8], stereoscopy method [7], and volume intersection method [2,3,5,13,18,19,21,22]. The first two methods use active illumination from sources such as a laser and grating light. The position of the light source must be adjusted precisely in order to achieve higher accuracy. The stereoscopy method uses passive illumination, i.e., the property of object reflection under an ambient lighting environment. However, it does not work well when the object has a uniform reflecting surface. The problem of

feature point correspondence would occur in the stereoscopy method. The volume intersection method uses a contour line to avoid the problem of feature point correspondence. However, the contour line cannot be used to represent the concave surface of an object.

In the present study, because the diamond-patterned surface of the router is very complicated and cannot be illuminated uniformly, we utilized a sequence of silhouette images of the router and extracted the upper contour edge to reconstruct a set of isograms. Such a set of isograms shows the features of the router surface. From each silhouette image, some information on the surface and some features of the router could be obtained. Because detailed information on the router is required, it is rotated at intervals of 1° and the silhouette image is obtained accordingly. Therefore, 360 silhouette images of each router are obtained. As the geometry of every good blade of the router is similar, the shapes of such blades on the isograms and blade patterns are also similar. These blade patterns can then be used to identify defects in the router. A survey of different methods employed for feature extraction analysis and classification is provided in [4]. Some methods that can be used to extract features for classification and pattern recognition are also included in [4].

3 AOI system

A diamond-patterned router has a diamond-cut geometry on the cylindrical surface that causes the surface to be a non-uniform reflecting surface. Theoretically, the track of each blade on a cylindrical router is formed by two oppositely directed helices and each blade has similar geometry. Such a feature of the blade inherently forms a specific pattern. Because collapse that occurs to some extent on the blades changes its appearance at different angles, a new approach is required to identify the collapse on such types of complicated surfaces. When the silhouette image of the router is obtained under an appropriate illumination environment, the peak and valley data of the silhouette image would become helpful for router collapse detection.

Based on the above concepts, an AOI system is devised for router collapse inspection. The hardware configuration is illustrated in Fig. 4. The proposed AOI system includes an LED backlighting system, an auto-controlled rotational fixture, a CCD camera (IDS-uEye CCD with 2,048 × 1,536 resolution), and a lens (1.5× magnification) with 56 mm working distance. Figure 5a shows the image of the router under an ambient lighting environment. Figure 5b shows an extracted silhouette image under the backlighting environment. The router is loaded in the fixture and rotated in intervals of 1° and a silhouette image is obtained. The flowchart of the proposed vision inspection method is given in Fig. 6. The details of this method are described below.

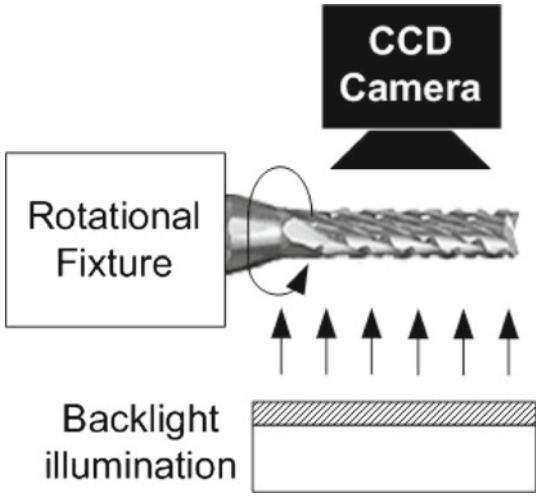

Fig. 4 Hardware illustration of the proposed router collapse auto-inspection system

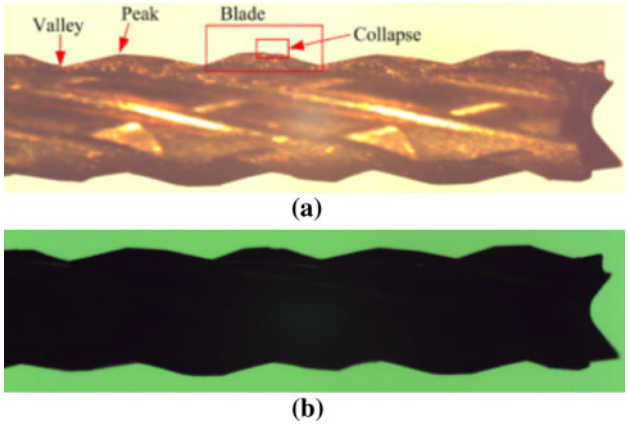

Fig. 5 **a** The image of a router grabbed under ambient lighting environment. The features of valley, peak and collapse of spiral blades are illustrated. **b** The silhouette image of a router grabbed under backlighting environment

3.1 Silhouette edge and extraction of associated features

To process and analyze each silhouette image, the origin of the image coordinate system is set at the upper left corner and the $[X, Z]$ coordinate system is adopted, as shown in Fig. 7. All the edge points on the upper silhouette edge of each silhouette image of the router are extracted on the basis of the 1D edge detection method [15]. This implies that each silhouette image is cut into a set of "slices" by scan lines perpendicular to the X axis from the left to the right of the silhouette image. A function $E(i)_j$ is defined to record the Z coordinate of the upper edge point of the ith slice of the silhouette image j, which is obtained when the fixture is turned at degree j. Hence, the $[X, Z]$ coordinates of all the edge points in the corresponding silhouette image can be recorded as $(i, E(i)_j)$. The value i ranges from 0 to a number, obtained by subtracting 1 from the width of the silhouette image, while j ranges

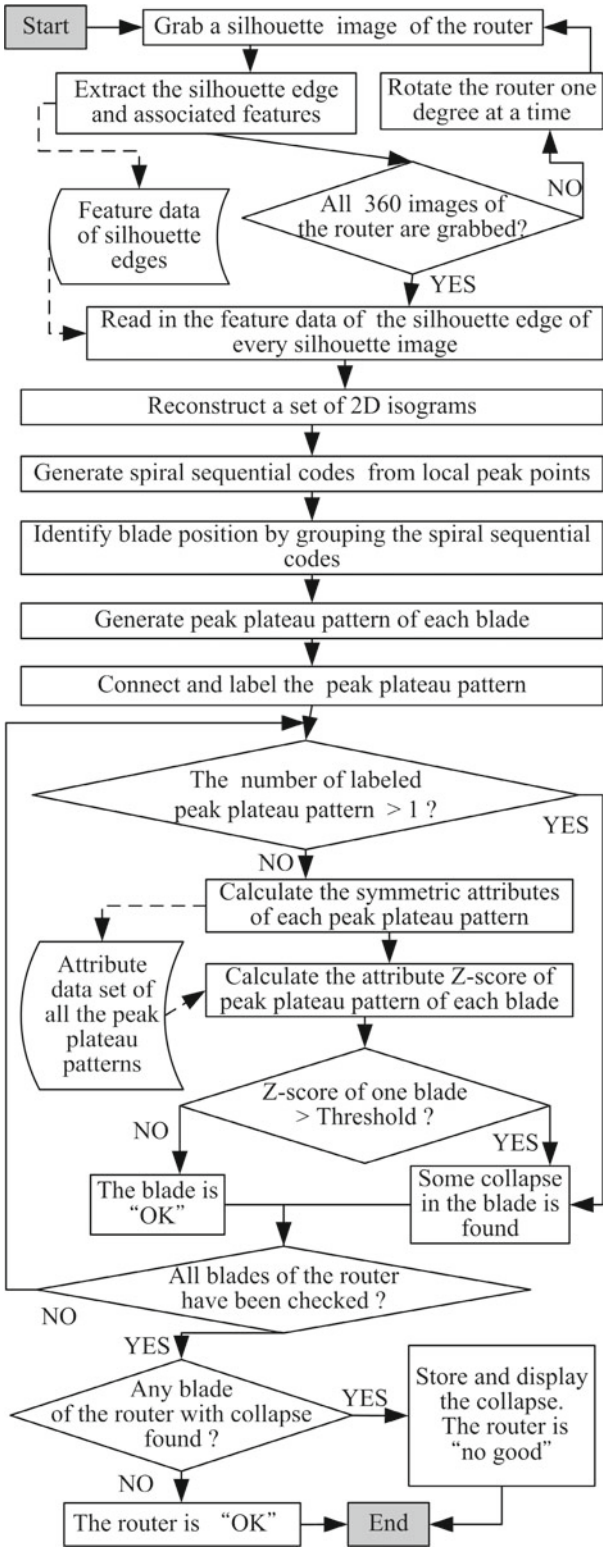

Fig. 6 The flowchart of proposed router collapse auto-inspection approach

from 0 to 359. First, the noise and unnecessary details in the silhouette image are removed by using the Gaussian smoothing operator (HIPR). Then, the edge point with the maximum

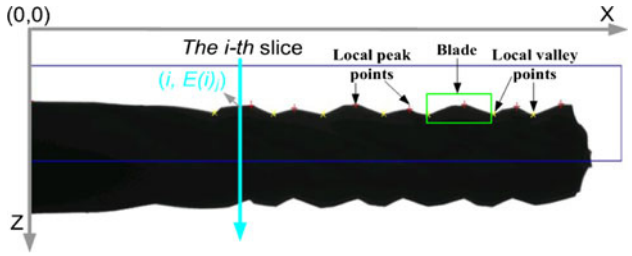

Fig. 7 Local peak and local valley points of the edge points of the silhouette image j grabbed when the router is rotated at degree j

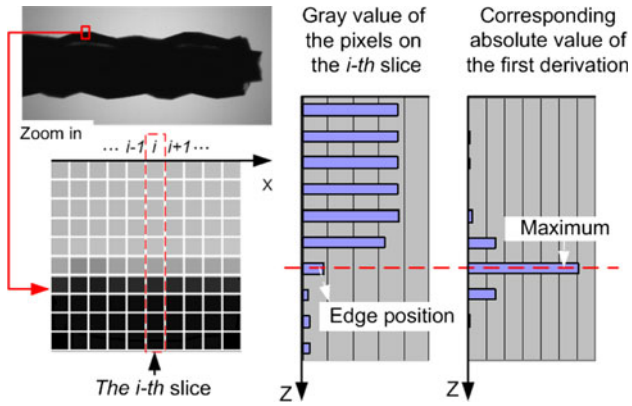

Fig. 8 The illustration of silhouette edge extraction method

amplitude is selected; this amplitude is the absolute value of the first derivative of the gray value of the slice, as shown in Fig. 8. The edge point with a local smaller Z value of each silhouette edge corresponds to a local peak point and is indicated by "+" in Fig. 7. Similarly, the edge point with a local larger Z value of each silhouette edge corresponds to a local valley point and is indicated by "×". The silhouette image between two nearest local valley points is the partial silhouette of the blade.

3.2 Reconstruction of 2D isograms

After extracting the upper edge points and the local peak and valley points from all the 360 silhouette images, we can set an associated $[X, Z]$ coordinate system for each silhouette image. We include another coordinate axis Y in the $[X, Z]$ coordinate system in order to integrate all the upper edge points of the 360 silhouette images. The Y axis is used to describe the obtained angle of all the 360 silhouette images. Hence, the shell of the router surface could be spread out on the $[X, Y, Z]$ coordinate system, as illustrated in Fig. 9. The points on the plane $Y = 0$ are the edge points of the silhouette image, which is obtained at 0°. All the edge points are recorded as $(i, j, E(i)_j)$; that is, each line that is perpendicular to the $[X, Y]$ plane contains one edge point.

Now, a set of 2D isograms is reconstructed, and it can be used to represent the simplified interwoven surface of

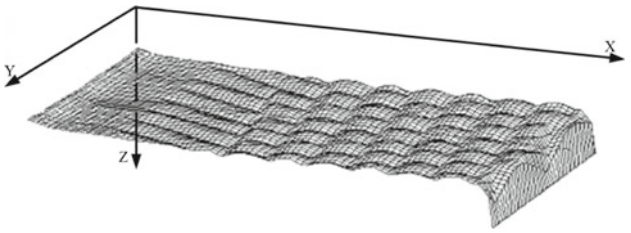

Fig. 9 Stripped and spread surface of a router

the blades of the router. In other words, the router surface is peeled off and spread out on a plane by subtracting the Z coordinate from the $[X, Y, Z]$ coordinate system and by transforming the Z coordinate data of the edge point into a gray value, as shown in Fig. 10a. In the above transformation, a higher gray value of the edge point corresponds to a lower Z coordinate. The discrete black and white points on the reconstructed isograms correspond to the local peak and valley points of the router, respectively; that is, the edge point $(i, j, E(i)_j)$ in the $[X, Y, Z]$ coordinate system is transformed into the point (i, j) in the 2D isograms ($[X, Y]$ coordinate system). Let $G(m, n)$ be the gray value of the point (m, n) on the reconstructed isograms. Min(E) and Max(E) are the minimum and maximum values of the Z coordinate, respectively, of all the edge points in the $[X, Y, Z]$ coordinate system. The set of 2D isograms is reconstructed according to the following equations:

$$G(m,n) = \mathrm{Max}(E) - E(m)_n + k, \quad \text{for } \mathrm{Max}(E) - \mathrm{Min}(E) = 255 \tag{1}$$

$$G(m,n) = \frac{255[E(m)_n - \mathrm{Min}(E)]}{[\mathrm{Max}(E) - \mathrm{Min}(E)]}, \quad \text{for } \mathrm{Max}(E) - \mathrm{Min}(E) > 255 \tag{2}$$

The parameter k is used to reconstruct the isograms with high visibility. The router is loaded without special alignment on the fixture. Therefore, one-third of the upper part of reconstructed isograms can be wrapped around its bottom part to obtain extended isograms, as shown in Fig. 10b. This allows us to represent each blade of the router as an entire blade in the extended isograms.

3.3 Generation of spiral sequential codes

In the reconstructed 2D isograms, any two tracks formed by connecting the local valley points form a quasi-hexagonal structure to represent a blade, because the upper and lower ends of the diamond pattern cannot be observed clearly. Such a quasi-hexagonal structure of a blade on the 2D isograms contains an s-like pattern (s-pattern) formed by the local peak points. This implies that the quasi-hexagonal structure nearly corresponds to a blade of the router. The collapse of the router blade can be identified by describing such s-patterns. Therefore, each s-pattern is numbered, starting from 1, in the sequence from the upper left to the lower right corners, as shown in Fig. 11. Although such a pattern represents a track of local peak points and would be helpful for router collapse inspection, the local peak points are discrete points and unsorted on the isograms; in other words, the s-patterns are unsorted. Hence, to number and describe each s-pattern, we assign a code known as spiral sequential code (SS-code) to each local peak point sequentially from the upper-left to the lower-right corners.

However, because the set of isograms is constructed by peeling off the router surface and spreading it on a plane, a geometrically complete blade such as that shown in s-pattern #7 in Fig. 11 is divided into two parts; that is, some local peak points of s-pattern #7 are separated into two parts on the isograms. In order to clearly explain the assignment of the SS-codes in this case, a simplified and enlarged illustration of the local peak points (black rectangle) and local valley points (white rectangle) of s-patterns #6 and #7 in Fig. 11 is provided in Fig. 12. The number in Fig. 12 is the sequence of the SS-code assigned to the local peak point. SS-codes #14 and #15 belong to the same blade. In Fig. 12, SS-codes #1–#12 are grouped together for identifying the position of s-pattern #6. The method for auto-grouping the SS-codes is described in Sect. 3.4.

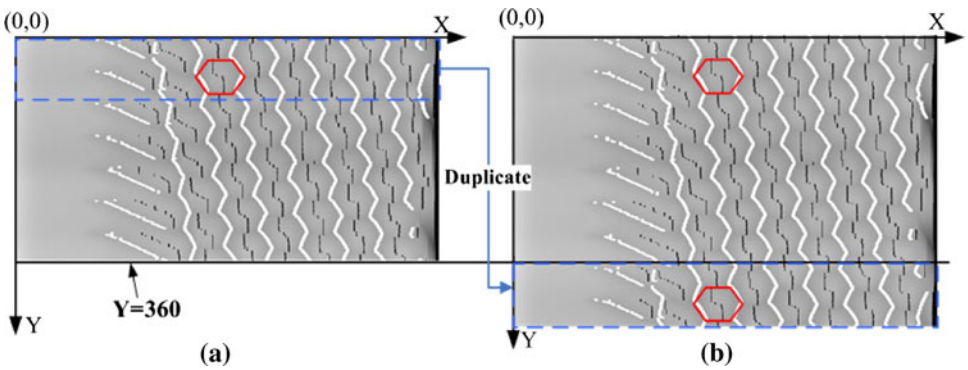

Fig. 10 **a** Reconstructed 2D isograms and **b** extended isograms formed by wrapping the upper one third isograms to the button, the local valley points (*white points*) and local peak points (*black points*)

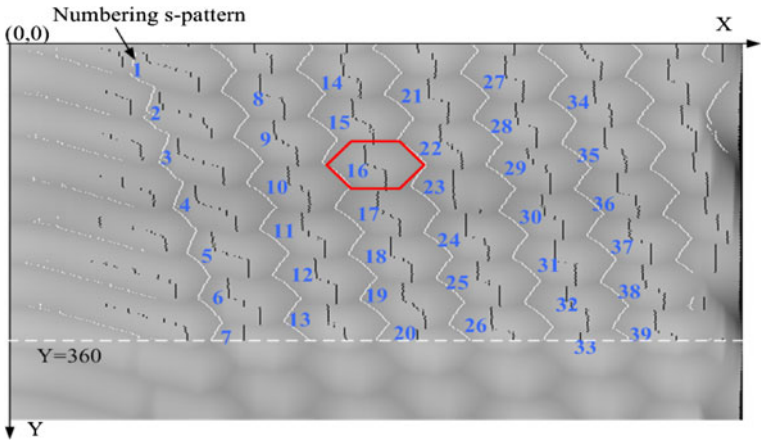

Fig. 11 The valley tracks of neighboring blades on the 2D isograms constitutes a quasi-hexagonal structure, The local peak points (*black*) will formed a s-pattern in each quasi-hexagonal structure

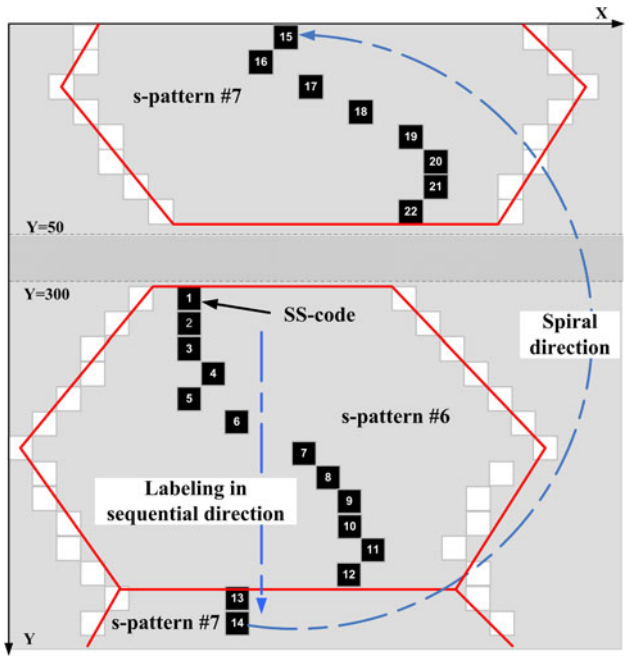

Fig. 12 The illustration of SS-code assigning

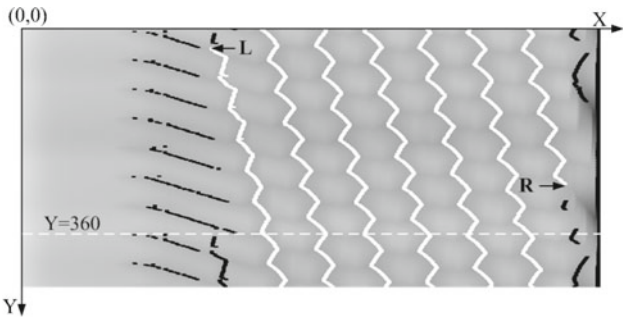

Fig. 13 The consecutive valley routes (*white*) obtained by dilating the originally discrete local valley points of the set of isograms

Before assigning the SS-codes, we must identify and label the starting and ending local peak points of the isograms as the first and last SS-codes, respectively. However, because the length and diameter of the router or even the angle of loading the router on the rotational fixture may be different, the positions of the starting and/or ending local peak point in the isograms shift randomly. Hence, a method that can identify and label the starting and ending local peak points automatically is proposed and described below.

Since the diamond-patterned blade of the router is constructed by different directional valley routes, the local valley points that can represent the partial valley routes are used to identify the starting and ending local peak points in the isograms. First, we utilize the image morphological dilation operation to connect the discrete local valley points into consecutive valley routes. The result of the dilation of the discrete local valley points is shown in Fig. 13 by consecutive white line segments. Second, each consecutive valley route is traced following the dilation result. Because the valley route after dilation is very evident, it can be used as the starting point of the valley route, located in the upper left corner, to identify and label the starting local peak point of the isograms. Similarly, the ending local peak point of the isograms in the lower right corner can be identified.

Let {Peaks} represent the set of all local peak points on the isograms. Let (L_x, L_y) and (R_x, R_y) represent the coordinate values of the starting point L and the ending point R of the valley route, respectively, as shown in Fig. 14. If $\{P\}$ represents a set of points, let $\mathrm{Min}_x(\{P\})$ and $\mathrm{Max}_x(\{P\})$ represent the minimum and maximum values of the X coordinates in $\{P\}$, respectively. Then, the starting local peak point S_p and the ending local peak point E_p can be identified using the following equations:

$$S_p = \mathrm{Min}_x(\{P\}), \text{ where}$$
$$P = \{\{\text{Peaks}\} \cap (Y = L_y) \cap (X > L_x)\} \quad (3)$$
$$E_p = \mathrm{Max}_x(\{P\}), \text{ where}$$
$$P = \{\{\text{Peaks}\} \cap (Y = R_y) \cap (X < R_x)\} \quad (4)$$

S_p and E_p identified using these equations are shown in Fig. 14. After obtaining the starting and ending local peak

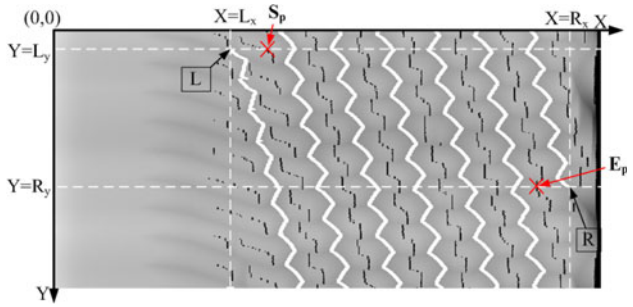

Fig. 14 The identified starting local peak point (Sp) and ending local peak point (Ep) according to the consecutive valley route (*white*)

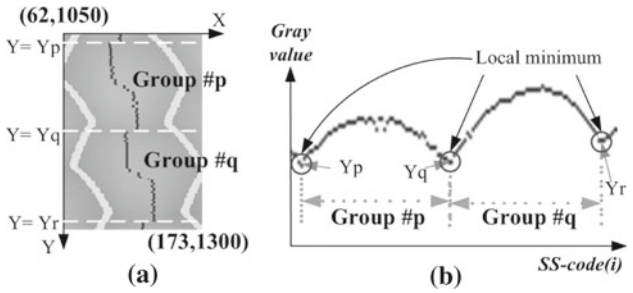

Fig. 15 **a** A portion of Fig. 14, **b** corresponding distribution of the gray value of the local peak points

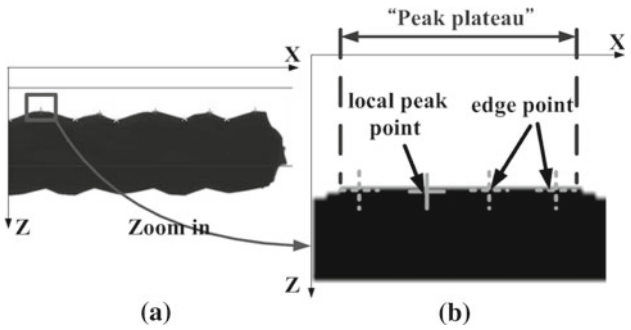

Fig. 16 The illustration of peak plateau. **a** Portion of silhouette image. **b** Edge points neighboring the local peak point have the same gray value is called "peak plateau"

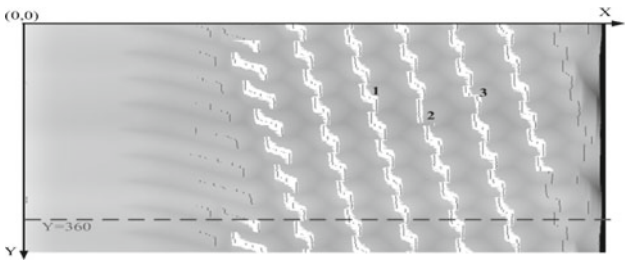

Fig. 17 Peak plateau (*white*), local peak points (*red*) of the isograms

points, the SS-code can be assigned from S_p to E_p in sequence in a spiral direction, as shown in Fig. 12. The SS-code generation method is explained in detail in Appendix A.

3.4 Blade identification by grouping of spiral sequential codes

After assigning the SS-codes to each local peak point, we can further classify them into several groups. Based on these groups, we can identify the position of each blade of the router. Because there are many blades, for simplicity, we consider an enlarged portion of Fig. 14, as shown in Fig. 15a. SS-codes with local minimum gray values could be used for SS-code grouping, as shown in Fig. 15b. Let $f(i)$ be the gray value function of SS-code(i). The local minimum of $f(i)$ is defined as follows:

$$\begin{aligned} &f(i^*) \text{ is a local minimum of } f(i), \text{ if there exists an} \\ &\text{SS-code}(i^*) \text{ for which } f(i^*) \leqq f(i), \\ &\text{for all SS-code}(i) \text{ with } |i - i^*| < \varepsilon. \end{aligned} \tag{5}$$

ε is an experimental parameter for obtaining a local minimum of $f(i)$ in the 2ε interval. Following Eq. (5), we could obtain the local minimum Yp, Yq, and Yr to classify the SS-codes into two groups—group #p and group #q—as shown in Fig. 15a. Similarly, all the SS-codes can be classified into proper groups. Each group that includes the set of associated local peak points nearly corresponds to a blade of the router.

3.5 Pattern analysis

In general, more than one neighboring point of the local peak point has the same Z coordinate value (height) as that of the local peak point, as illustrated in Fig. 16. A set of neighboring edge points forms a "peak plateau." For example, the peak plateau observed in the isograms in Fig. 14 is shown in Fig. 17. Because each group of SS-codes includes a set of local peak points, it also corresponds to a peak plateau pattern. Therefore, the peak plateau pattern can be used to evaluate the accuracy of a blade. The peak plateau pattern of a good blade shows connectedness and symmetry. A connected peak plateau is formed by the edge points that are connected together to form a single element, while a symmetric peak plateau is formed by edge points that form a symmetric pattern. As illustrated in Fig. 18, s-pattern #1 represents a good blade and has a connected and symmetric peak plateau pattern, while s-pattern #2 represents a collapsed blade whose peak plateau pattern shows poor connectedness. S-pattern #3 represents a collapsed blade whose peak plateau pattern shows poor symmetry. The connectedness and symmetric properties are the two critical features for peak plateau pattern analysis.

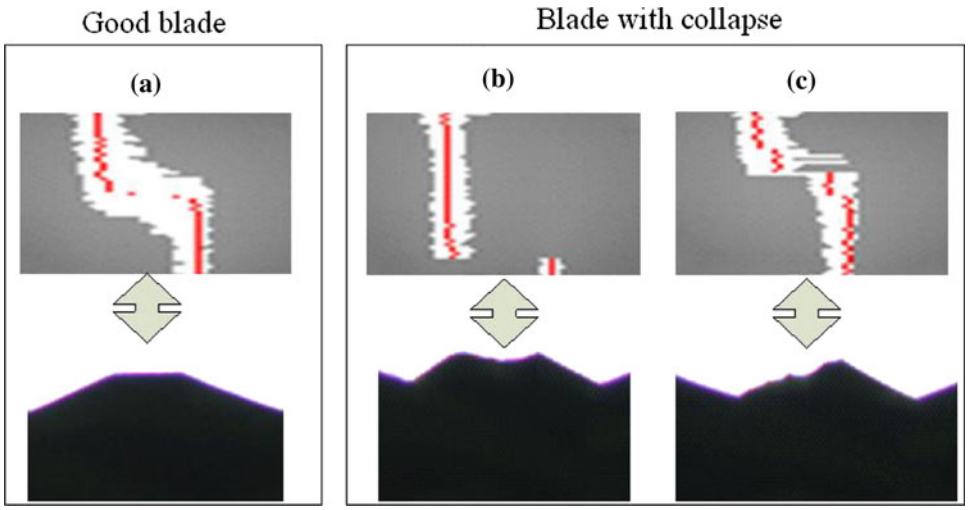

Fig. 18 Illustrations of partial silhouette image of a router and its corresponding peak plateau pattern. **a** Good blade, **b** collapsed blade with poor connectedness, **c** collapsed blade with poor symmetry

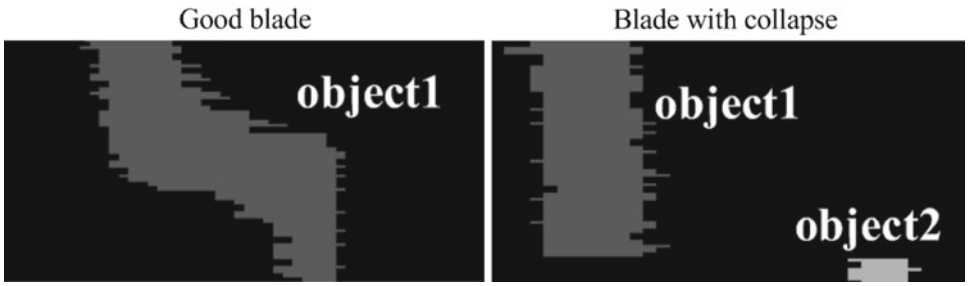

Fig. 19 Connected pattern analysis

3.5.1 Connected pattern analysis

When the peak plateau pattern of a blade is not connected, it is separated into several objects due to the collapse. To detect this type of collapse, we use the method of "connected object labeling" to count the number of objects in each peak plateau pattern, as shown in Fig. 19. The process of analyzing the connectedness of each peak plateau pattern is described as follows:

A. If two points in the peak plateau pattern are connected based on 8-neighbor connectivity, then they are considered to be part of the same object.
B. If more than one object exists in the peak plateau pattern, then collapse has occurred on the blade to some extent.

3.5.2 Symmetric pattern analysis

When the peak plateau pattern of a blade is both connected and symmetric, the blade is identified as a good blade. Due to the symmetric property, we use quadrantal moments [6] as attributes for peak plateau pattern analysis. Each peak plateau pattern has a symmetric attribute value of quadrantal moments. If the symmetric attribute value of a peak plateau pattern is an outlier among all the symmetric attribute values, the blade corresponding to this peak plateau pattern is a collapsed blade. Nowadays, as the yield rate of the router is greater than 60%, we assume that most blades of the router are normal blades. Moreover, if a collapsed blade is detected based on the connectedness property of the peak plateau pattern, it would not be inspected based on the symmetric property. Hence, a Z-score method [16] is adopted to detect the outlier of the symmetric attribute values of the peak plateau patterns of the blades. The process of analyzing the symmetric property of each peak plateau pattern is described as follows:

A. The minimal bounding rectangle, which is parallel to the coordinate axis, of each peak plateau pattern is obtained. The geometric center (x_0, y_0) of this rectangle is calculated, as shown in Fig. 20. Based on this geometric center, the minimal bounding rectangle is divided into four quadrants.
B. Let (x, y) be a point in the peak plateau pattern and $G(x, y)$ be its gray value. Q_k denotes the quadrantal moments of each quadrant k, $1 \leqq k \leqq 4$, and D_{ij} denotes the product of the x moments of the ith order and the y moments of the jth order. The quadrantal moments are

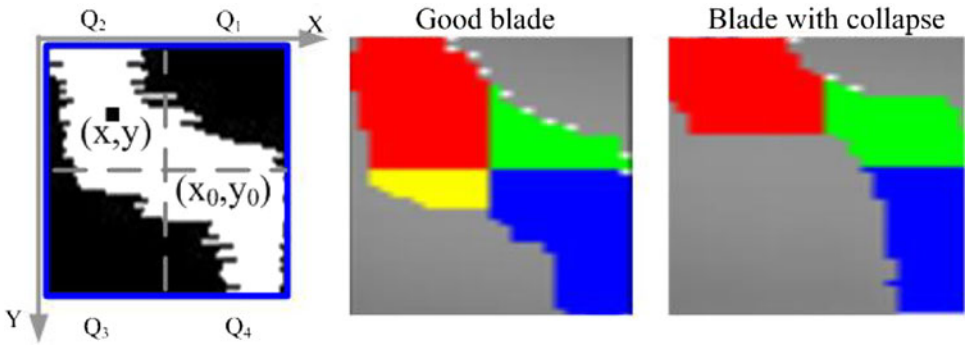

Fig. 20 symmetric pattern analysis of the peak plateau pattern of a router blade

calculated using Eq. (6):

$$Q_k D_{ij} = \sum_{(x,y)\in Q_k} (x - x_0)^i (y - y_0)^j G(x, y), \quad \text{where } i \geq 0,\ j \geq 0,\ 1 \leq k \leq 4. \tag{6}$$

C. The symmetric property of each peak plateau pattern can be determined by the symmetric attribute values P1 and P2 by using the following equations.

$$P1 = \text{ABS}(Q_2 D_{00} - Q_4 D_{00}) \tag{7}$$

$$P2 = \text{ABS}((Q_2 D_{22} + Q_3 D_{22}) - (Q_1 D_{22} + Q_4 D_{22})) \tag{8}$$

$P1$ is defined as the absolute difference between the sum of gray value of Q_2 and Q_4. The smaller the value of $P1$, the higher is the symmetry of the peak plateau pattern. $P2$ is defined as the absolute difference between the second-order quadrantal moments of $(Q_2 + Q_3)$ and $(Q_1 + Q_4)$. As in the case of P1, the smaller the value of $P2$, the higher is the symmetry of the peak plateau pattern.

D. From Sect. 3.4, we obtain the positions of all the inspected blades on the isograms. Using Eqs. (7) and (7), we obtain two sets of symmetric attribute values of n inspected blades of the router. Let $P1_1, P1_2, \ldots, P1_n$ represent a set of n blades with P1 symmetric attribute values, and let $P2_1, P2_2, \ldots, P2_n$ represent a set of n blades with $P2$ symmetric attribute values. The Z-score used for detecting the outlier from the two sets of symmetric attribute values is calculated using Eqs. (9)–(14) as follows:

$$\text{For}\, P1,\ Z1_i = \frac{P1_i - \overline{P1}}{S1}, \quad i = 1, 2, \ldots, n \tag{9}$$

where

$$\overline{P1} = \frac{P1_1 + P1_2 + \cdots + P1_n}{n} \tag{10}$$

$$S1 = \frac{1}{n}\left(\left|P1_1 - \overline{P1}\right| + \left|P1_2 - \overline{P1}\right| + \cdots + \left|P1_n - \overline{P1}\right|\right) \tag{11}$$

$$\text{Similarly, for}\, P2,\ Z2_i = \frac{P2_i - \overline{P2}}{S2}, \quad i = 1, 2, \ldots, n \tag{12}$$

where

$$\overline{P2} = \frac{P2_1 + P2_2 + \cdots + P2_n}{n} \tag{13}$$

$$S2 = \frac{1}{2}\left(|P2_1 - \overline{P2}| + |P2_2 - \overline{P2}| + \cdots + |P2_n - \overline{P2}|\right) \tag{14}$$

From the definition of the Z-score, a value in a set whose z-score is greater than 3 or less than -3 significantly varies from the other values in the set. Such a value can be identified as an outlier. However, because the Z-scores of $P1$ and $P2$ are positive in this study, we must only identify the outliers with Z-scores greater than 3. Hence, two rules for collapsed blade detection can be derived as follows:

If $Z1_i > T1$, then collapse has occurred on blade(i).
Or,
If $Z2_i > T2$, then collapse has occurred on blade(i).

$T1$ and $T2$ are two parameters for symmetric pattern analysis and are determined by experimentation.

4 Experimental results and discussion

In this section, we present some experimental results of router collapse inspection and the performance of the proposed AOI

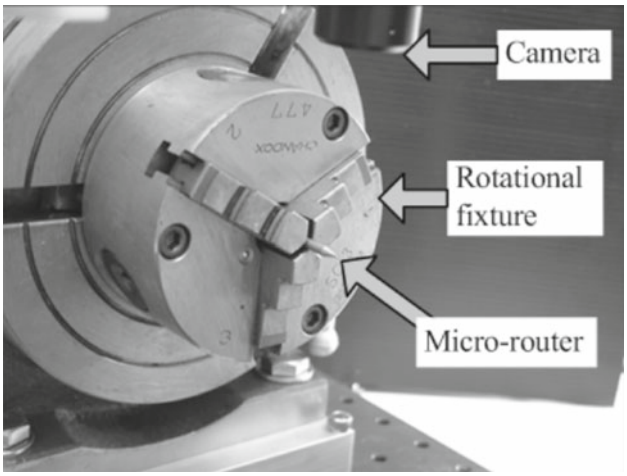

Fig. 21 The prototype of the AOI system for router collapse inspection

system. Figure 21 shows an image of the prototype of the proposed AOI hardware system. Two types of routers with different diameters are used in this inspection experiment. 15 routers of each type are used to verify the accuracy and robustness of the proposed AOI system. The inspection time for each router is approximately 220 s, including the time required for rotating it by 360° at intervals of 1°.

Some data computed by experimentation are provided in Table 1, including the number of connected objects and the Z-scores of $P1$ and $P2$ of a sample router with a diameter of 1.0 mm. S-pattern #21 and #27 in the first column of Table 1 that are indicated in bold type are the collapsed blades identified by human inspectors. The values in the other three columns, including the number of connected objects and the Z-scores of $P1$ and $P2$, are calculated by following the proposed methods. The inspection data of two other routers obtained similarly are provided in Tables 2 and 3. Note that #of s-pattern indicated in bold type in Tables 2 and 3 are the collapsed blade identified by human inspectors.

In Table 1, the number of connected objects of s-pattern #21 is 2; this implies that there are two separated objects in the peak plateau pattern. According to the proposed connectedness property of the peak plateau pattern, the blade associated with s-pattern #21 is identified as a collapsed blade. Hence, the Z-scores of $P1$ and $P2$ of s-pattern #21 are ignored and are indicated by "*" in Table 1. S-pattern #11 in Table 3 is identified similarly.

For the remaining two attributes of the Z-score, any Z-score data of $P1$ and $P2$ greater than +3 would be an extremely large outlier. If both thresholds $T1$ and $T2$ are set as 3 in Table 1, then the Z-score of $P1$ of s-pattern #27, which is 4.54, indicates that the blade associated with s-pattern #27 is identified as a collapsed blade, according to the proposed peak plateau symmetric property. Similarly, the blades associated with s-pattern #14, s-pattern #17, and s-pattern #23 in Table 2 are identified as collapsed blades. In Table 3, the Z-score of $P1$ of s-pattern #12 is 3.24, which indicates a collapsed blade; in reality, however, this blade is not a collapsed blade.

Therefore, a "false alarm" occurs. This indicates that the value of $T1$ is possibly very small and must be adjusted. Hence, we perform some experiments to determine a reason-

Table 1 The experimental detail of a sample router #1 with diameter = 1.0 mm

# of s-pattern	# of connected object	Z-score of $P1$	Z-score of $P2$
1	1	−0.27	1.03
2	1	−0.93	−0.27
3	1	−1.58	−1.57
4	1	−1.05	0.86
5	1	−0.51	−1.82
6	1	−0.43	−1.7
7	1	−0.83	−1.56
8	1	−0.83	1.24
9	1	0.08	0.53
10	1	1.42	1.36
11	1	1.59	1.23
12	1	2.11	1.41
13	1	−0.09	−0.53
14	1	−1.46	−0.15
15	1	−1.61	0.69
16	1	−0.72	−0.98
17	1	1.08	1.29
18	1	1.79	1.34
19	1	0.22	0.88
20	1	0.18	0.17
21	2	*	*
22	1	−1.48	0.04
23	1	1.35	1.27
24	1	−0.15	−1.31
25	1	0.32	−1.07
26	1	−0.94	−2.18
27	1	4.54	1.48
28	1	1.08	0.13
29	1	−0.24	−0.17
30	1	0.49	1.42
31	1	−0.02	0.99
32	1	2.04	1.39
33	1	−1.49	−0.59
34	1	−1.41	−2.27
35	1	−0.64	−0.09

Bold entries indicate a blade is the collapsed blades and identified by human inspectors beforehand. *Asterisks* indicate if a blade is defined as collapsed blade by the proposed connectedness property, the Z-scores of $P1$ and $P2$ of the blade is ignored

Table 2 The experimental detail of a sample router #2 with $d = 1.0$

# of s-pattern	# of connected object	Z-score of $P1$	Z-score of $P2$
1	1	−1.54	0.27
2	1	−1.12	1.33
3	1	−1.37	−0.66
4	1	−1.64	−0.28
5	1	−1.19	−0.38
6	1	−1.7	−0.56
7	1	−0.92	0.86
8	1	−1.04	−1.78
9	1	0.05	−0.45
10	1	0.3	1.14
11	1	−0.29	0.54
12	1	0.31	1.34
13	1	0.43	−1.35
14	1	4.52	1.68
15	1	−0.16	−0.72
16	1	−0.95	−0.38
17	1	4.11	1.76
18	1	−1.09	−2.12
19	1	0.35	−0.25
20	1	−0.77	−2.2
21	1	−0.41	−1.89
22	1	0.27	−0.34
23	1	4.61	1.76
24	1	−1.19	−1.76
25	1	−0.27	0.98
26	1	−0.01	0.88
27	1	0.02	0.58
28	1	0.79	1.11
29	1	−0.08	0.57
30	1	0.49	−1.17
31	1	−1.23	−0.91
32	1	−0.31	−0.31
33	1	−0.25	0.97
34	1	0.48	1.1
35	1	0.77	0.64

Bold entries indicate a blade is the collapsed blades and identified by human inspectors beforehand

Table 3 The experimental detail of a sample router #10 with $d = 0.8$

# of s-pattern	# of connected object	Z-score of $P1$	Z-score of $P2$
1	1	−1.06	0.62
2	1	0	0.66
3	1	0.72	1.03
4	1	−1.35	−1.46
5	1	−0.21	−2
6	1	−0.87	−1.91
7	1	1.33	0.92
8	1	0.89	1.04
9	1	0.56	0.58
10	1	2.36	1.73
11	2	*	*
12	1	3.24	−1.69
13	1	−1.72	0.37
14	1	0.75	2.25
15	1	−1.09	−0.91
16	1	0.37	−0.46
17	1	−1.33	1.79
18	1	0.29	1.32
19	1	0.93	0.19
20	1	0.13	−0.31
21	1	−1.56	−2.1
22	1	0.11	−0.17
23	1	−1.1	−1.49
24	1	−1.73	0.2
25	1	2.69	1.5
26	1	−0.3	−0.31
27	1	−0.43	0.9
28	1	0.9	0.06
29	1	−1.06	0.62

Bold entries indicate a blade is the collapsed blades and identified by human inspectors beforehand. *Asterisks* indicate if a blade is defined as collapsed blade by the proposed connectedness property, the Z-scores of $P1$ and $P2$ of the blade is ignored

able range of values for $T1$ and $T2$. First, $T2$ is set to 3, and then we inspect all the 30 routers by increasing $T1$ from 3 to 4.5. We calculate both the number of false alarms and the number of missed detections for every pair of $T1$ and $T2$. Figure 22 shows the trend of both the number of false alarms and the number of missed detections against the threshold value of $T1$. $T1$ is increased from 3 to 4.5 in this experiment. The number of false alarms reaches a stable value of 19 when $T1$ is greater than 3.8, while the number of missed detections reaches a stable value of 3 when T1 is less than 4.1. From Fig. 22, for stable inspection performance of the proposed AOI system, $T1$ can be set in the range of 3.8–4.1. After similar experimentation, the trends of both the number of false alarms and the number of missed detections against the threshold value of $T2$ become stable, as shown in Fig. 23. $T2$ can be set in the range of 3–3.5.

Therefore, if we set $T1 = 4$ and $T2 = 3$, then the peak plateau of the collapsed blades of sample router #1 (Table 1) can be indicated by a white rectangle, as shown in Fig. 24. S-pattern #21 has a poor connectedness property, while s-pattern #27 has a poor symmetric property. The experimental data of all the 30 routers are listed in Table 4. Although the successful detection rate for different diam-

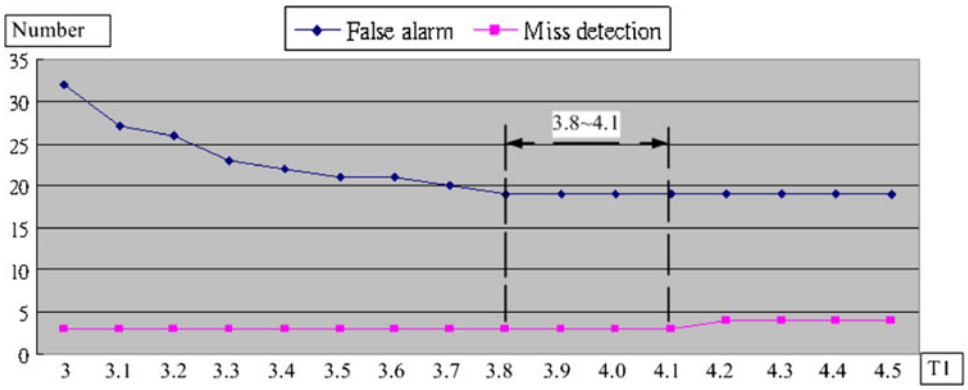

Fig. 22 The trend of both the number of false alarm and the number of miss detection against the setting of the threshold value $T1$

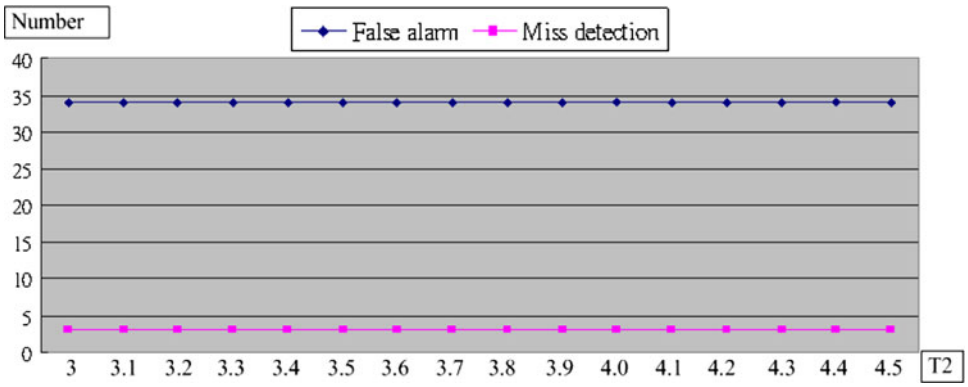

Fig. 23 The trend of both the number of false alarm and the number of miss detection against the setting of the threshold value $T2$

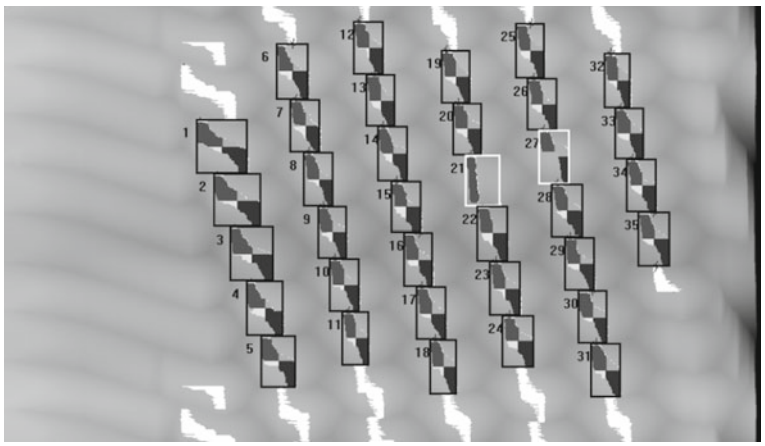

Fig. 24 The peak plateau of the blades with collapse was marked in *white rectangles*

eters is greater than 96%, the problem of false alarm must be solved in the proposed system. Figure 25 shows a few examples of collapse and the corresponding positions on the blades. Figure 25 also demonstrates that most false alarms are caused by small particles. The particles affect the peak plateau pattern of the blade. S-pattern #1 represents a normal blade. S-patterns #5 and #6 represent normal blades with particles on them and are falsely detected. S-patterns #2, #3, and #4 represent collapsed blades and are successfully identified. However, because the geometry of a blade on the tail of the router is different from those of the other blades, the proposed system still cannot detect collapses such as No.9 of the type 2 router. This type of tail collapse increases the number of missed detections.

5 Conclusions

In this paper, an AOI system that can identify the collapse of a diamond-patterned micro-router is presented. The physical collapsed area would be 0.01 mm^2 only on the complicated surface of the diamond-patterned router. It is difficult for human inspectors to detect collapse in such a small area. The proposed AOI system utilizes silhouette feature extraction

Table 4 The experimental results ($T1 = 4$, $T2 = 3$, D = diameter)

No. of router	# of blades in each router		Blade with collapse		# of collapse detected		# of false alarm		# of miss detection	
	$D = 1.0$	$D = 0.8$	$D = 1.0$	$D = 0.8$	$D = 1.0$	$D = 0.8$	$D = 1.0$	$D = 0.8$	$D = 1.0$	$D = 0.8$
1	35	28	2	0	2	0	0	0	0	0
2	35	27	3	0	3	0	0	0	0	0
3	35	27	0	0	0	1	0	1	0	0
4	35	26	0	0	0	0	0	0	0	0
5	37	25	2	1	2	4	0	3	0	0
6	36	27	0	0	0	0	0	0	0	0
7	35	27	1	0	2	1	1	1	0	0
8	38	27	0	1	1	1	1	0	0	0
9	36	27	1	1	2	1	1	1	0	1
10	36	29	1	1	1	1	0	0	0	0
11	36	27	0	1	2	1	2	1	0	1
12	36	28	0	0	1	1	1	1	0	0
13	35	41	0	1	1	2	1	2	0	1
14	36	27	0	1	0	1	0	0	0	0
15	36	35	0	0	1	1	1	1	0	0
	537	428	10	7	18	15	8	11	0	3

Type 1 routers: Diameter = 1.0, successful detection rate = 0.985. Type 2 routers: Diameter = 0.8, successful detection rate = 0.967

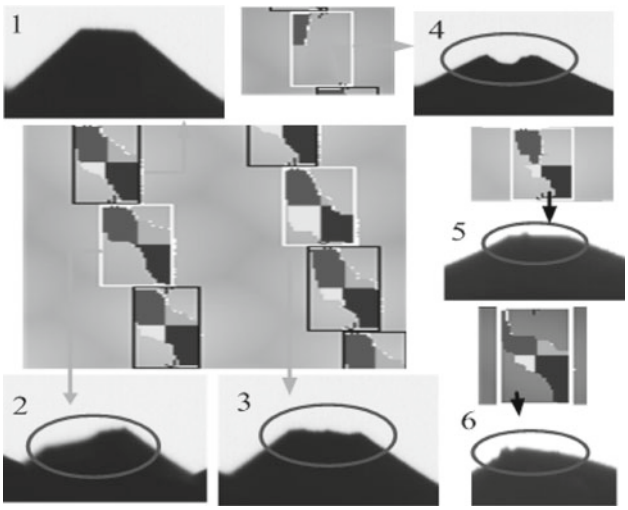

Fig. 25 The experimental results and corresponding partial silhouette images

and surface reconstruction to reconstruct the peeled-off 2D isograms of the router. Based on the reconstructed 2D isograms, this system can identify the 3D defect of the router. The successful detection rate for different diameters is greater than 96%. The proposed AOI system can assist in determining the quality of routers. In future study, we aim to improve the rotational mechanism and refine the inspection algorithm in order to increase the inspection speed for production line synchronous inspection. Moreover, the proposed approach is not suitable for inspecting the collapse in the tail part of a micro-router. A new solution is required for this purpose.

Appendix A

Let {Peaks} and {Valleys} be the set of all local peak points and local valley points, respectively.

Algorithm 1: SS-code generation

Input: {Peaks}, {Valleys}, starting local peak point S_p, ending local peak point E_p

Output: SS-code of a router (isograms)

Method:

/* Search each local peak point in the isograms along the spiral direction and assign an SS-code to it.*/

i = 0 /* i: used for generating SS-code*/

/*Assign an SS-code from the starting local peak point S_p */

B_x = X coordinate value of S_p, B_y = Y coordinate value of S_p

Assign SS-code (i) to point (B_x, B_y mod 360).

Do

i = i + 1, j = 0 /* j: used for finding the local valley point from {Valleys}.*/

Do /*Search the local valley point from {Valleys} for the starting point. This point is also used for searching the next local peak point from {Peaks}.*/

j = j + 1

Until point ($B_x - j$, ($B_y + 1$) mod 360) $\subset$ {Valleys}

/* Point ($B_x - j$, ($B_y + 1$) mod 360) is the starting point which is used for searching the next local peak point from {Peaks}.*/

k = 0 /* k: used for searching the next local peak point from {Peaks}.*/

Do /* Search the next local peak point from {Peaks}; then assign the succeeding SS-code */

$$k = k + 1$$

If the point $(B_x - j + k, (B_y + 1) \bmod 360) \subset \{Peaks\}$ **and** the point $(B_x - j + k, (B_y + 1) \bmod 360)$ has not been assigned an SS-code **then**

Assign SS-code (i) to the local peak point $(B_x - j + k, (B_y + 1) \bmod 360)$.

B_x = X coordinate value of SS-code (i).

B_y = Y coordinate value of SS-code (i).

Exit Do /*Exit this loop, search the next local peak point.*/

End If

Until point $(B_x - j + k, (B_y + 1) \bmod 360) \subset \{Valleys\}$

Until B_x = X coordinate value of E_p **and** B_y = Y coordinate value of E_p

/*Stop assigning SS-codes when the ending local peak point is encountered*/

References

1. Boehler, W., Marbs, A.: 3D scanning instruments. In: Proceedings of the CIPA WG6 International Workshop on Scanning for Cultural Heritage Recording. Corfu, Greece (2002)
2. Chen, H.H., Huang, T.S.: A survey of construction and manipulation of octrees. CVGIP **43**, 409–431 (1988)
3. Carr, J.C., Fright, W.R., Gee, A.H., Prager, R.W., Dalton, K.J.: 3D shape reconstruction using volume intersection techniques. In: Proceedings of the Sixth International Conference on Computer Vision, pp. 1095–1100 (1998)
4. Costa, L., Cesar, R.: Shape Analysis and Classification. Chemical Rubber Company Press, Boca Raton (2001)
5. Fuchs, H., Kedem, Z.M., Uselton, S.P.: Optimal surface reconstruction from planar contour. Commun. ACM **20**, 693–702 (1977)
6. Flusser, J., Suk, T., Saic, S.: Recognition of blurred images by the method of moments. IEEE Trans. Image Process. **5**, 533–538 (1996)
7. Fua, P.: From multiple stereo views to multiple 3D surfaces. Int. J. Comput. Vis. **24**, 19–35 (1997)
8. Hu, G., Stockman, G.: 3D surface solution using structure light and constraint propagation. IEEE Trans. PAMI **11**, 390–402 (1989)
9. Hinds, K., Treanor, G.M.: Analysis of stresses in microdrills using the finite elements method. Int. J. Mach. Tools Manuf. **40**, 1443–1456 (2000)
10. Hazra, L., Kato, H., Kiryu, T., Hashimoto, Y., Kuroda, T., Tsuchiya, Y., Sakuma, I.: Inspection of reground drill point geometry using three silhouette images. J. Mater. Process. Technol. **127**, 169–173 (2002)
11. HIPR. http://www.cee.hw.ac.uk/hipr/html/hipr_top.html
12. Kuang, C.C.: Intelligent microdrill inspection system. M.Sc. thesis, National Taiwan University of Technology (2000)
13. Laurentini, A.: How far 3D shapes can be understood from 2D silhouettes. IEEE Trans. PAMI **17**, 188–195 (1995)
14. Laser Design. http://www.laserdesign.com
15. Marr, D., Hildreth, E.: Theory of edge detection. Proc. R. Soc. Lond. Ser. B Biol. Sci. **207**, 187–217 (1980)
16. Mendenhall, W., Beaver, R.J., Beaver, B.M.: Introduction to Probability and Statistics. Duxbury Press, North Scituate (2005)
17. Perng, D.B., Hung, C.Y., Chen, Y.C.: An AOI system for microdrill measurement. In: Proceeding of 18th International Conference on Production Research. Salerno, Italy (2005)
18. Szeliski, R.: Rapid octree construction from image sequences. CVGIP Image Underst. **58**, 23–32 (1993)
19. Srivastava, S.K.: Octree generation from object silhouettes in perspective views. CVGIP **49**, 68–84 (1990)
20. Union Tool. http://www.uniontool.com
21. Yemez, S.Y.: 3D color object reconstruction from 2D image sequences. Proc. ICIP **3**, 65–69 (1999)
22. Zheng, J.Y.: Acquiring 3D models from sequences of contours. IEEE Trans. PAMI **16**, 163–177 (1994)

Author biographies

Dr. Der-Baau Perng is currently a Processor and the Director of Manufacturing Management Center, Department of Industrial Engineering and Management (IE&M), National Chiao Tung University (NCTU). He received the BS, MS, and Ph.D. degrees all in Computer Engineering from NCTU. He joined the Department of IE&M, NCTU from 1988. He was the Chairman of the Department (1991–1994, 2006–2009), the Director of Production System Automation Research Center (1995–1996), the Executive Manager of NCTU Spring Foundation (1998–1999), the Director of Alumni Communication Center (1998–2000), the Director of Semiconductor Manufacturing Management Center (1997–2001), and the Secretary-in-Chief of NCTU (2003–2007). His current research interests include Computer Vision, CAD/CAM Integration, E-Commerce, and Supply Chain Management.

Yen-Chung Chen received his PhD degree in Industrial Engineering and Management, National Chiao Tung University, Taiwan, in 2008. Currently, he is a postdoctoral researcher at Opto-mechatronics Technology Center, National Taiwan University of Science and Technology, Taiwan. His current research interests include image processing, computer vision and automatic optical inspection.